

Towards a 3D Vision System based on Single-Pixel imaging and indirect Time-of-Flight for drone applications

Carlos Alexander Osorio Quero
Electronics Department
Instituto Nacional de Astrofísica,
Óptica y Electrónica (INAOE)
Puebla, Mexico
caoq@inaoep.mx

Daniel Durini Romero
Electronics Department
Instituto Nacional de Astrofísica,
Óptica y Electrónica (INAOE)
Puebla, Mexico
ddurini@inaoep.mx

Ruben Ramos-Garcia
Optical Department
Instituto Nacional de Astrofísica,
Óptica y Electrónica (INAOE)
Puebla, Mexico
rgarcia@inaoep.mx

Jose de Jesus Rangel-Magdaleno
Electronics Department
Instituto Nacional de Astrofísica,
Óptica y Electrónica (INAOE)
Puebla, Mexico
jrangel@inaoep.mx

Jose Martinez-Carranza
Computer Science Department
Instituto Nacional de Astrofísica,
Óptica y Electrónica (INAOE)
Puebla, Mexico
carranza@inaoep.mx

Abstract— In this paper, a theoretical analysis of a vision system for 2D/3D single-pixel imaging using principles of compressed sensing and Indirect-Time-of-flight measurements is presented. The goal is to use this system for autonomous drone navigation in environments with adverse conditions where typical sensors used by RGB or RGB-Depth cameras typically fail. The harsh environments considered include smoke, rain, or fog. The performance evaluation is based on the signal-to-noise ratio considering different levels of background illumination, measured depths oscillating between 1 m and 10 m, different percentages of object reflectivity, and finally, the achievable spatial resolution understood as the standard deviation of the distance measured for a particular object in the illuminated scene under a set of defined border conditions. For the vision system proposed, we consider active illumination consisting of an array of NIR LEDs emitting Hadamard illumination patterns, and a pulsed laser diode used for Indirect-Time-of-flight. We propose using an InGaAs NIR sensitive photodiode as a single-pixel detector. Since the proposed vision system will be mounted on a drone, parameters such as weight, dimensions, power consumption, and processing time were considered to maximize its efficiency.

Keywords—Single-pixel imaging (SPI), time-of-flight (TOF), InGaAs, 2D/3D Imaging, CUDA, GPU, Orthogonal Matching Pursuit (OMP), compressed sensing, Hadamard patterns

I. INTRODUCTION

Commercial CMOS vision systems, besides offering a vast amount of signal processing systems and analog-to-digital converters (ADC) on-a-chip, they are very reliable, reasonably cheap, and compact. However, these systems exhibit several limitations if applied in Time-of-Flight (TOF) 3D imaging and ranging applications. For instance, the systems based on silicon solutions continuously have to deal with very high background photon shot noise, mostly if used outdoors. Also, due to the silicon radiation bandwidth normally ranging between 400 nm and 1000 nm (ultra-violet (UV), visible (VIS), and near-infrared (NIR) parts of the

spectra) at the most; exactly the main emission bandwidth of the Sun at ground level, and also the bandwidth where the maximum allowed the light intensity of the active illumination source required for TOF principle-based systems is mostly diminished due to the international IEC Eye Safety regulation IEC62471 for Class 3R lasers [1]. Besides, conventional RGB or RGB-depth sensors are limited under low visibility conditions, such as in the rain, fog, smoke, or snow-impregnated scenarios that hinder the image acquisition or estimate the distance between the camera system and the different objects in the illuminated scene. For drone applications, depth information has been proven relevant in autonomous navigation applications [2]. Nevertheless, such sensing limitations prohibit the deployment of drones in scenarios with adverse conditions mentioned.

Motivated by the above, we propose a vision system that can operate under extreme background illuminations working conditions. For this, we propose using a vision system working at longer wavelengths than those achievable by silicon-based systems. The latter enables taking advantage of the bandwidth window yielding much higher atmospheric absorption and thus much lower background illumination, using active illumination sources with higher irradiances allowed by the ESR, and the fact that using longer NIR wavelengths diminishes Rayleigh and other scattering mechanisms. Thus enables propagation of active illumination in the rain, smoke, fog, or snow. As there are no image sensors fabricated with InGaAs, sensitive to emitted radiation in the range around 1550 nm can allow the TOF sensor functionality commonly pursued in CMOS based solutions. We propose using commercially available single InGaAs photodiodes accompanied by the SPI principle of operation to generate 3D images at near video rates. For the latter, we present a mathematical model that considers different photon and electrical noise sources of the proposed system, a maximum

100 Klux background light intensity, and consider three different sets of goal parameters: i) distance of objects in the illuminated scene varying between 1 m and 10 m; ii) different reflectivity indexes of the objects evaluated in the illuminated scene, and iii) spatial resolution, i.e., the standard deviation of the evaluated distances between the different objects in the illuminated scene and the vision system proposed, calculated considering the time that the emitted light pulse requires to reach the different objects in the scene, be reflected by them, and travel back to the detector system allocated aside the active illumination source. Thus, we propose a vision single-pixel imaging [1] system working in combination with the principle of Indirect-Time-of-flight (iToF) [3, 4, 5]. We are confident that this vision system has the potential to be exploited in drone applications involving autonomous navigation.

For evaluating the proposed vision system, we defined a methodology for testing the devices and the implemented algorithms in the vision system at near video rate, and the generation of 2D and 3D images. The first analysis makes a comparative study considering the InGaAs Thorlab FGA015 diode. For this work, we have focused on determining the minimum integration time of the diode to capture an image under different noise conditions and different object reflection coefficients at different distances. This parameter is decisive for calculating the video frame rate performance, measured in frames per second (fps). The second analysis is related to the required processing time of the single-pixel generated signals enabling the creation of 2D images. Because the image generation system operates using the single-pixel principle, we use the OMP algorithm [15] to recover and reconstruct 2D images. For the implementation of the OMP algorithm, an initial analysis is carried out to determine the minimum amount of patterns used to generate grayscale images with a compression factor of 2% for different resolutions (64x64, 64x16, 128x16, and 256x16 “virtual” pixels). We assessed the OMP algorithm in two different architectures, namely CPU and GPU, to determine the image processing time. The previously described analysis enables us to calculate the frame rate (fps) of two different generated images' resolutions. A third analysis is related to the implementation of the TOF system for the generation of 3D images. This process will operate in parallel to the image capturing process. We consider the implementation of the continuous wave (CW) ITOF [6] and IEC Eye Safety regulation IEC62471 standard applied to Class 3R lasers [1] to define the required performance specifications of the photodetector at the level of distance measurement accuracy. The latter analysis defines the expected spatial resolution under different noise levels and different reflection coefficients of the target materials.

II. MODELLING OF THE SPI-ITOF VISION SYSTEM PROPOSED

Since the vision system proposed is spi-based [7], we provide a brief description of the sensing approach's main concepts. Sequences of structured light (for example, Hadamard patterns [7]) are projected over the object, and the reflected light is focused onto a photodetector with no

spatial information. The object is reconstructed from the photodetector's electrical output signal using the OMP algorithm [15] to recover the 2d image.

As a first step, we select the most suitable photodetector for intensity measurements. We chose a nir-sensitive photodetector ($1544 < \lambda < 1556$ nm) to reduce the background light illumination since the sun's spectral radiation content is small in this range. Regarding the properties of the objects embedded in the illuminated scene, we assume the usual lambert reflection model shown in fig. 1.

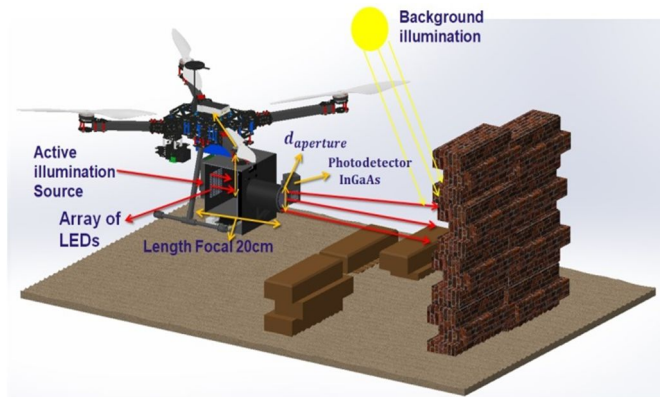


Fig. 1. Scheme of measurement of energy level detected, the source of noise from the background lighting, distance, stages of the optical system are considered.

A key factor here is the assessment of the minimum integration time required by the chosen photodiode under different working conditions, i.e., the time required to capture the photons emitted by the array of LEDs that get reflected by the objects in the scene, and finally reach the photodiode and provide an electrical signal above the background noise. For the determination of the integration time, we use (1), which models the number of photons arriving at the single-pixel [8]. Considering the use of a band-pass filter in front of the chosen photodiode, (1) depends on the spectral content $1544 \text{ nm} < \lambda < 1556$ nm, the detector quantum efficiency $QE(\lambda)$ in this bandwidth, the length of the integration time of the detector T_{int} , and pixel's effective photosensitive area A_{pix} , defined as $A_{wxl} FF$, where A_{wxl} is the semiconductor window and FF the photodiode's fill-factor (FF). The number of photons $E(N)$ impinging the photodetector photoactive will depend on the irradiance of the active light source (the array of chosen LEDs) and the ambient light conditions, as well as on the distance of the object to be detected and the optical parameters that define its reflective surface (see Fig. 1). In (1), the parameter $\Phi_{e\lambda}$ is defined as the irradiation level of the active source, $E_{e\lambda_sun}(\lambda)$ irradiation level of the sun illumination considered to be of 100 klux, the $f_{\#}$ number $f_{\#} = f_{fo}/d_{aperture}$ is the focal distance/opening distance, h is Planck's constant = $6.62607004 \times 10^{-34} \text{ m}^2 \text{ kg/s}$, z is the measured distance, c is speed of light constant, τ the lens transmittance, ρ the material reflection index, and α_{FOV} the focal aperture angle [6] of the emitting LED array. Table 1 summarizes the values of the different quantities considered for simulation purposes.

$$E(N) = \int_{\lambda_1}^{\lambda_2} \frac{\rho \tau_{lends} Q E(\lambda) T_{int} A_{pix} FF \lambda}{4 h c f_{\#}^2} \left[\frac{\Phi_{e\lambda}}{\pi z^2 \tan(\alpha_{FOV})} + E_{e\lambda_sun} \right] d\lambda \quad (1)$$

TABLE I
PARAMETER EVALUATION OF InGaAs DIODE

Parameter	InGaAs diode Thorlab	
	FGA015	
Windows Pixel Area mm ²	0.0707	
Power Source radiation (Leds NIR)	25.6 W	
Distance range	10 m	
Reflectance range	[0.2 0.5 0.8]	
Background illuminance		100 klux
Optical bandpass filter	1544 nm - 1556 nm	
Total transmittance of optics	0.9	
Field of view	20°	
f-number	0.95	
Fill Factor (FF)	35 %	

After the algorithm was defined before was applied, the evaluation of InGaAs diode Thorlab FGA015 [13] using the parameters defined in Table I was performed. We made sweeping of the integration time starting from an initial time off to reach the maximum distance for which the InGaAs diode FGA015 is not affected by the noise floor, see Fig. 2.

Calculate time integration:

In order to calculate the minimum integration time required to detect each of the emitted Hadamard patterns properly, the analysis procedure is as follows:

1. Take the initial parameters of the optical system, as listed in Table 1.
2. Calculate the number of overall number of photons $E(N)$ impinging the photodetector photoactive area using (1) and considering background illumination in the wavelength range defined by the narrow band-pass filter added to the used active illumination.

3. Calculate the overall electrical noise floor in terms of the variance σ_{Noise_floor} calculated as the square-root of the sum of squares of the background illumination photon shot noise variance σ_{ph} , the variance representing the statistical variation in the amount of thermally generated electrons within the InGaAs photodetector or the dark shot noise σ_{dark} , and the read-noise σ_{read} generated by the readout electronics, as expressed by (2).

$$\sigma_{Noise_floor} = \sqrt{(\sigma_{ph})^2 + (\sigma_{dark})^2 + (\sigma_{read})^2} \quad (2)$$

4. Define the maximum distance reached $Z_{measurement}$ for the minimum level condition where the $E(N)$ is affected for the noise.

$$\left| E(N) - \sigma_{Noise_floor} \right| < \delta_{th}$$

5. If $Z_{measurement} < Z_{max}$ for a reflection index ρ the integrate time T_{int} is increased the skip to step 3. If $Z_{measurement} \approx Z_{max}$ then $T_{inti} = T_{inti-1}$ condition of the stop.

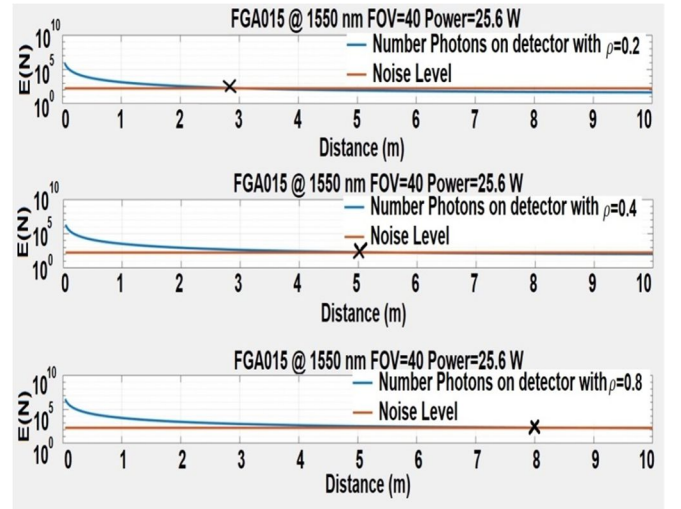


Fig. 2. Behavior of the Thorlabs FGA015 InGaAs photodiode in function of numbers photons detected, and the noise floor, for the integration time proposed, considering different reflection indices and the distances measured.

A. Processing algorithm implemented to SPI reconstruction

Single image processing time is a critical factor for the generation of 2D digital images and video streams in SPI for application in real-time eg. Drone navigation. To reduce the time required by the 2D image processing system, we determined the minimum number of illumination patterns equivalent to a compression factor of 2% to be able to adapt the Batch-OMP algorithm [8] based on hardware architecture and a GPU. The Batch-OMP algorithm [8], in comparison with another compressing sensing (CS) algorithm as OMP and Cholesky-OMP, presents improvement in processing time due to that don't make

operations of the inverse matrix, on the contrary, is used the definition of the Gram-matrix, $G = \Phi^T \Phi$, where initially is needed to make a pre-calculated Gram-matrix G with an initial projection i , where an initial projection as $p^0 = \Phi^T y$ is defined this allows finding the new atom $\Phi_{:,i}$, that will be used as stop criterial for the system solution calculation.

Algorithm 1: Batch-OMP algorithm [15]

Batch OMP algorithm input data: Dictionary Φ , input signal y , target sparsity K

Batch OMP algorithm output data: sparse representation x that fulfills the relation $y \approx \Phi x$

Detailed algorithm sequence:

```

1: set  $I = \{0\}$ ,  $L = [1]$ ,  $p^0 = \Phi^T y$ ,  $\varepsilon = y \cdot y^T$ ,  $i = 1$ ,  $G = \Phi^T \Phi$ 
2:  $p = p^0$  # Initial projection
3: while ( $\varepsilon_{i-1} > \varepsilon$ ) do
4:    $k = \arg \max_k |p|$  # Finding the new atom  $\Phi_{:,i}$ 
5:   if  $i > I$  then # Cholesky update
6:      $w = \text{Solve for } w \{L_{i-1} w = G_{i-1, k}\}$ 
7:     # Update of the Cholesky decomposition
8:      $L_i = \begin{bmatrix} L_{i-1} & 0 \\ w^T & \sqrt{1 - w^T w} \end{bmatrix}$ 
9:   end if
10:   $I = (I, k)$  # Support update
11:   $x_i = \text{Solve for } c \{L L^T x_i = p^0\}$ 
12:   $\beta = G x_i$  # Matrix-sparse-vector product for each path
13:   $p = p^0 - \beta$ 
14:   $\delta^k = x_i^T \beta$  # Calculate error
15:   $\varepsilon^k = \varepsilon^{k-1} - \delta^k + \delta^{k-1}$  # Calculate normal error  $\varepsilon$ 
16: end while

```

For the implementation of the Batch-OMP algorithm we defined 4 kernels that must operate in parallel [9-10-15]:

i. In the first kernel, the input information is defined, the Gram-matrix ($G = \Phi^T \Phi$) is generated (line 1 of the Algorithm 1: Batch-OMP algorithm), and the residual norm r is calculated.

ii. The second kernel was used to calculate the new atom $\Phi_{:,i}$ (line 4 of the Algorithm 1: Batch-OMP algorithm)

iii. The third kernel was used to calculate the Cholesky decomposition (lines 6 and 7 of the Algorithm 1: Batch-OMP algorithm), where the matrix $N \times N$ was defined to calculate the matrix L (see (3) [11]).

$$L_{new} = \begin{bmatrix} L & 0 \\ w^T & \sqrt{1 - w^T w} \end{bmatrix} \quad (3)$$

iv. The fourth kernel was used to calculate the matrix space-vector product (line 11 of the Algorithm 1: Batch-OMP algorithm), and also to calculate the normal error e (line 14 of the Algorithm 1: Batch-OMP algorithm [15]).

B. Image processing time analysis

We implemented the Batch algorithm (see algorithm 1) as much in GPU Jetson nano as CPU i5, and we compared

the processing time for a different image size of 64×64 , 64×16 , 128×16 , and 256×16 and calculated the frame rate, see figure 3.

In the test, we can determine that the Batch-OMP algorithm implemented on the GPU platform ran 2.7 times faster than when it was implemented using the CPU based platform. This will be a factor determination for applications in real-time. The processing time would be between 20 to 30 ms with which we can have a video frame rate of the 24 fps.

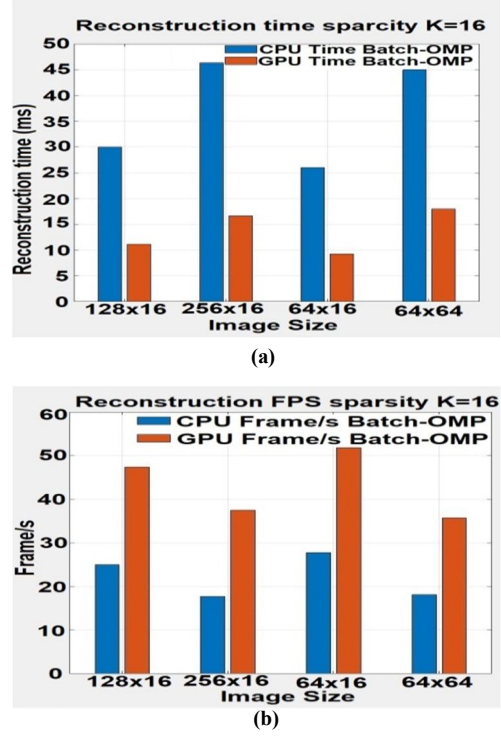


Fig. 3. Performance evaluation results obtained for the Standard-OMP and Batch-OMP algorithms, respectively, running on the i5 CPU and the Jetson Nano GPU [10] platforms: (a) image reconstruction time required for the sparsity factor $k = 16$; (b) frames per second (fps) obtained for the results shown in a).

An example of a reconstructed image using the Batch-OMP algorithm with a size of 64×64 virtual pixels is shown in Fig. 4. The original image is shown in Fig. 4(a), in Fig. 4(b) reconstructed image with a sparsity value of $k = 16$ with a PSNR level of ~ 24 dB.

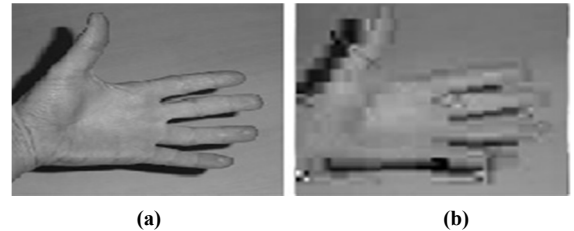


Fig. 4. An example of a reconstructed image with a size of 64×64 virtual pixels, reconstructed using the Batch-OMP algorithm running on the GPU platform: (a) original image deconstructed down to a size of 64×64 pixels; (b) reconstructed image with a sparsity value of $k = 16$.

C. Evaluation of indirect time-of-flight (iToF) measurement methods

As the 3D image reconstruction method, we use the reference distance measurement following the continuous-wave principle of time of flight indirect (CW-iToF [2-3]). The proposed approach estimates the depth of objects and scenarios using the reference distance as a complement of the shape-from-shading (SFS) [12], which will be used for estimate depth in the image 2D by single-pixel and generate the image 3D. To determinate the maximum measuring ranges with a spatial resolution below 1 cm. We evaluated the resolution capacity of the CW-iToF method over conditions of outdoors background illumination intensity ranging between 50 and 100 Klux on the one hand and on the other hand, indoor conditions with background illumination between 15 and 30 Klux. In the evaluation, we considered the reflectivity coefficient of the object in the illuminated scene to be 0.2, 0.5, and 0.8, respectively, for a system using 1,000-period continuous-wave NIR LED illumination at first and then expanding the number of accumulations (and improving the signal averaging feature) to 10,000 signal periods. The minimum amount of accumulations required is defined by the target spatial resolution of the system, the background illumination photon shot-noise, the distance of the target objects to the photodetector, and the reflection index of the materials covering these objects. To calculate the achieved spatial resolution, i.e., the standard deviation $\sigma_{CW-iToF}$ of the measured distance using the iToF method, we use (4) [6]. Where d_{max} corresponds to the maximum measurement distance, AR corresponds to the number of photons detected in the detector window, B corresponds to background noise, where $x=T_{TAP}/T_p$ is a scaling factor that depends on the pulsed time T_p and sample time T_{TAP} .

(4)

$$\sigma_{CW-iToF} = \frac{d_{max}}{A_R} \sqrt{\frac{A_R + 2B}{N_{acc}}} \frac{1}{2\pi F(x)}$$

The results obtained from the evaluation of the indirect distance estimation method are shown in Fig. 5. For the maximum measured distance (in meters) with a standard deviation (spatial resolution) of below 1 cm, estimated under different operating conditions. For the underwent evaluation, we considered the Thorlabs FGA015 InGaAs photodiode [13] over different conditions of the illumination in outdoor as for indoor considering different reflection indexes for the case of 10,000 (see Fig. 5(a)) and 1,000 (see Fig. 5(b)) period accumulations using a laser Thorlabs L1550P5DFB [14] with a pulse of a 65 ns in the wavelength of 1550 nm.

To determine maximum measurement distance with a resolution of below 10 mm, we modeling under indoor illumination conditions, using as elements photodetector the InGaAs diode Thorlab FGA015 [13], which enables measuring distances of between 0.8 and 4.3 m and under outdoor background illumination conditions, the measured distance range achieving spatial resolutions of below 1 cm was of between 0.3 and 1.5 m.

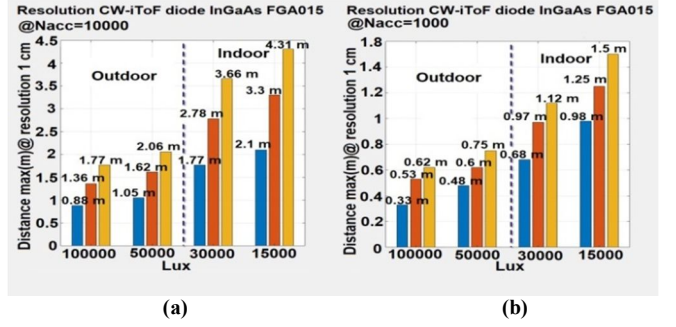


Fig.5. Maximum distance resolution (standard deviation in distance measurements) achieved using the CW-iToF method considering different reflection indices blue $\rho=0.2$, red $\rho=0.4$ and yellow $\rho=0.8$ of the objects and the Thorlabs FGA015 InGaAs photodiode [9] for (a) 10,000 illumination CW period accumulations and different background illumination levels, and (b) 1,000 illumination CW period accumulations and the same different background illumination levels.

III. PROPOSED SPI-ITOF VISION SYSTEM

Based on the analysis described in the previous section, we proposed a vision system for the generation of 2D / 3D and video images, shown in Fig. 6a and 6b. Three stages form this vision system: the first stage combines the lighting system active formed by an array of LEDs NIR in the wavelength of 1550 nm and projecting the pattern light over the object. The reflected light is catching for the photodetector module, which has an InGaAs photodiode Thorlab FGA015 [13], fig 7a. The second stage is the responsibility of processing the signal captured by the photodiode module through the use of an ADC, which is controlled by the GPU unit. The GPU unit is also responsible for a generation of the sequence of the Hadamard patterns, as well as the processing of converted data by the ADC, that will be used by the Batch-OMP algorithm running in the GPU unit to generate the 2D image. The third stage is responsible for generating the 3D image for which is need the combine the lasers pulsed array L1550P5DFB @1550 nm [14], disposed of at an angle of 90 grads over the photodetector module. The signals lasers are generated using the driver laser that is controlled by the GPU unit. The signals of lasers are projected sequentially over the object that wants to generate a 3D image, and the reflected signals of the lasers are catching by the photodiode, which is located in the photodetector module, fig7b. The lasers light signals are processed by the ADC. The converted data is used to make an estimation of the phase and calculate the distance references that will be used in combination with a shape-from-shading algorithm [12] (SFS) in the GPU unit for generating the 3D images (see (5) [6]).

(5)

$$d_{ref} = \frac{c \Delta\phi}{2 \pi f}$$

$$\Delta\phi = \arctan\left(\frac{C_3 - C_1}{C_0 - C_2}\right)$$

$$A = \frac{1}{2} \sqrt{(C_3 - C_1)^2 + (C_0 - C_2)^2}$$

$$B = \frac{1}{4}(C_0 + C_1 + C_2 + C_3)$$

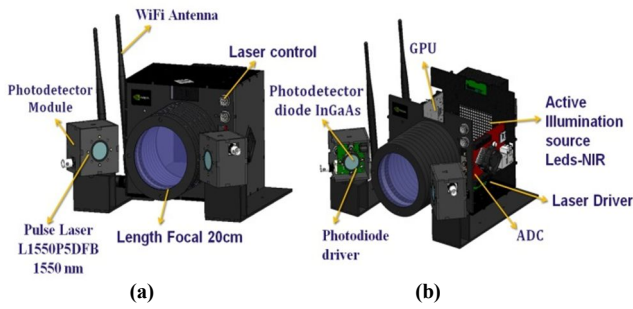


Fig.6. The proposed vision system dimension 11x12x13 cm , weight 1.3kg and power consumption 25W, a) front part elements module photodiode, focal lens with length focal 20 cm, Wi-Fi antenna, b)internal part elements GPU unit, ADC, active illumination source, photodiode driver ,photodetector diode InGaAs.

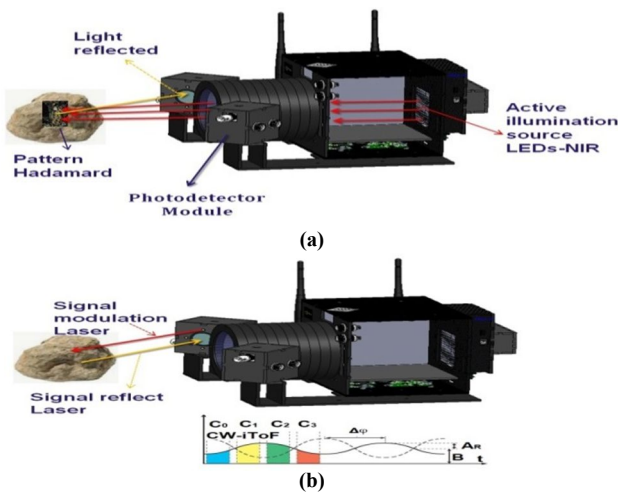


Fig.7. Vision system operation, a) patterns project Hadamard using the active illumination source LEDs-NIR and capture of the light reflected by the photodetector module, b) generation of the modulation signal of the laser and signal reflect the laser, which will be sampling to estimate the $\Delta\phi$ phase difference and calculate the reference the distance.

IV. CONCLUSION

In this paper, we have presented a theoretical analysis of the design of an SPI-iTOF Vision System. For the analysis of the vision system, we have proposed a methodology divided into three stages. The first stage regarded the selection of components based on background noise and distance resolution conditions. In this assessment, we determined that it is possible to use the photodiode Thorlab FGA015 to capture images for distances between 0.8 to 5 m , with a resolution of 1 cm, for objects with a refractive index of [0.2 0.5 0.8]. From this result, we are confident that the vision system has the potential to be exploited in drone applications in both indoor and outdoor environments. In the second stage, we implemented the Batch-OMP algorithm for 2D image generation, and we made the comparison of the processing time for CPU and GPU, the architectures with a sparsity $k=16$, and we got a reconstruction time between 20 and 30 ms, thus enabling a frame around 24 fps. In the third stage, we proposed implementing the method for generation imagen 3D that works in combination with the indirect-time-of-flight for calculating the reference of the distance used by the shape-

from-shading algorithm [12] (SFS) to the generation of image or map 3D.

REFERENCES

- [1] Laser Safety Facts. (Accessed Oct. 2019). [Online]. Available: <https://www.lasersafetyfacts.com/laserclasses.html>
- [2] J. Martinez-Carranza, L. Oyuki Rojas-Perez, A. A. Cabrera Ponce, R. Munguia-Silva. "Combining Deep Learning and RGBD SLAM for Monocular Indoor Autonomous Flight". 15th Mexican International Conference on Artificial Intelligence (MICAI). Guadalajara, Jalisco, Mexico. October, 2018.
- [3] D. Stoppa et al., "A CMOS 3-D imager based on single photon avalanche diode," IEEE Trans. Circuits Syst. I, Reg. Papers, vol. 54, no. 1, pp. 4–12, Jan. 2007.
- [4] C. Niclass, C. Favi, T. Kluter, F. Monnier, and E. Charbon, "Single-photon synchronous detection," IEEE J. Solid-State Circuits, vol. 44, no. 7, pp. 1977–1989, Jul. 2009.
- [5] S. Bellisai, F. Guerrieri, and S. Tisa, "3D ranging with a high speed imaging array," in Proc. Conf. PRIME, Jul. 18–21, 2010, pp. 1–4.
- [6] D. Bronzi, Y. Zou, F. Villa, S. Tisa, A. Tosi and F. Zappa, "Automotive three dimensional vision, a single-photon counting SPAD camera", IEEE Trans. Intell. Transp. Syst., vol 17, no. 3, pp. 782–795, Mar. 2016.
- [7] A.Süss. "High Performance CMOS Range Imaging", Ph.D. Thesis, University of Duisburg-Essen, Duisburg, DU, 2014.
- [8] R. Rubinstein, M. Zibulevsky and M. Elad "Efficient implementation of the k-svd algorithm using batch orthogonal matching pursuit". Cs Technion, 40(8):1–15 (2008).
- [9] J. Wang, M. Gupta, A. C. Sankaranarayanan "Lisens - a scalable architecture for video compressive sensing," in 2015 IEEE International Conference on Computational Photography (ICCP), pp. 1–9 (2015).
- [10] A. Borghi, J. Darbon, S. Peyronnet, T. F. Chan, S. Osher, "A simple compressive sensing algorithm for parallel many-core architectures", J. Signal Process. Systems, 71, 1–20 (2013).
- [11] H. Zhu, G. Yang and W. Chen "Efficient Implementations of Orthogonal Matching Pursuit Based on Inverse Cholesky Factorization", IEEE 78th Vehicular Technology Conference (VTC Fall), Las Vegas, NV, 2013, pp. 1-5 (2013).
- [12] L. Jin, R. Aimin and Z. Jingnan, "3D Reconstruction by Perspective Shape from Shading Using Linearized Triangular Element Surface Model," International Conference on Mechatronics and Automation, Luoyang, Henan, 2006, pp. 1763-1768 (2006).
- [13] <https://www.thorlabs.com/thorproduct.cfm?partnumber=FGA015>, last visited on August 11, 2020.
- [14] <https://www.thorlabs.com/thorproduct.cfm?partnumber=L1550P5DFB>, last visited on August 11, 2020.
- [15] O.Carlos, D.Daniel, R.Rubén, R. José and M.Jose, "Hardware parallel architecture proposed to accelerate the orthogonal matching pursuit compressive sensing reconstruction", Proceedings Volume 11396, Computational Imaging V, 113960N, (2020).